Supporting Information

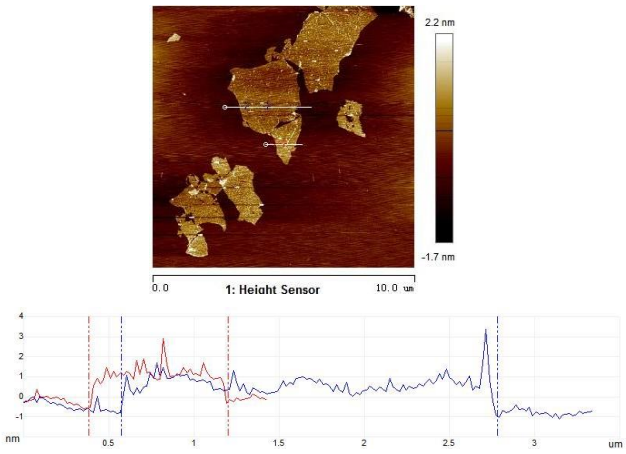

Fig. S1 AFM image and the height profiles of GO.

GO sheets have lateral sizes in the range of 2-5 μm, and heights of about 1 nm corresponding to a single layer of GO.

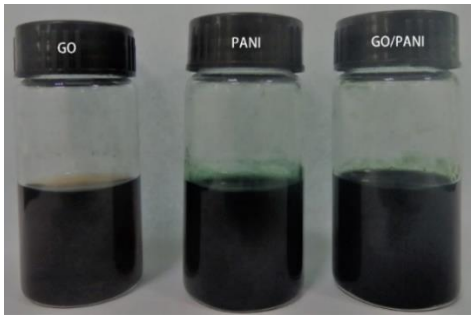

Fig. S2 Digital photos of the GO, PANI and GO/PANI solution.

PANI nanofibers dispersed with GO sheets to form a homogeneous aqueous suspension.

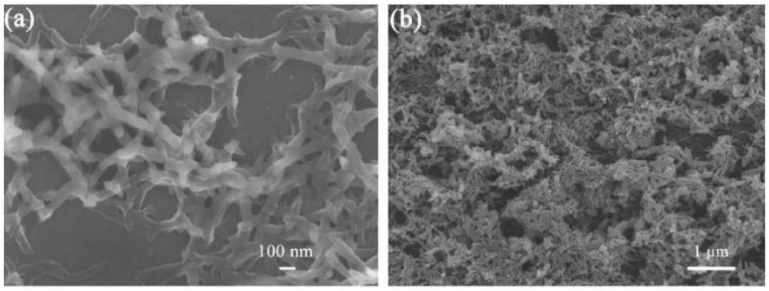

Fig. S3 SEM images of (a) PANI, (b) PANI/CNT film.

Without GO sheets in the suspension, we found that PANI nanofibers alone cannot be homogeneous coated onto CNTs

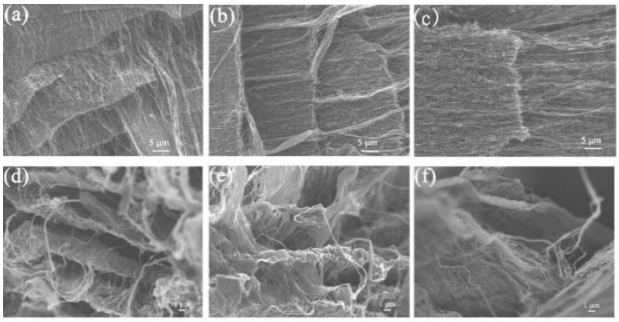

Fig. S4 SEM images of the 20%-PANI/GO/CNTs (a, d), 50%-PANI/GO/CNTs (b, e) and 80%-PANI/GO/CNTs (c, f) composite films.

In the SEM images of the 20%-PANI/GO/CNTs, 50%-PANI/GO/CNTs and 80%-PANI/GO/CNTs composite film, it was observed that a uniform layer-by-layer structure of the PANI/GO and CNT layer stacks was formed in the composite films. At the fractured region where the CNT and GO layers are flipped or tilted, the thickness of individual GO/PANI layers could be estimated to be about 0.2 μm and 0.6 μm for 20%-PANI/GO/CNTs, 50%-PANI/GO/CNTs composite film, respectively. For the 80%-PANI/GO/CNTs composite film with increasing PANI, the layered structure gradually diminished.

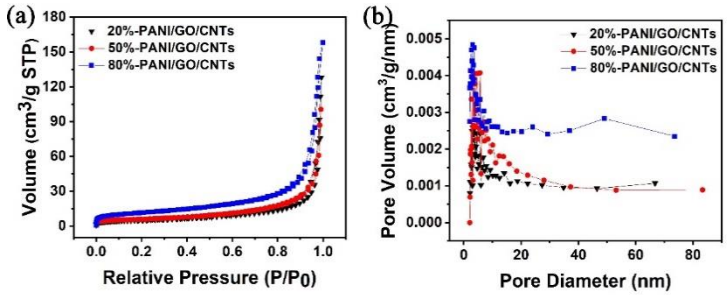

Fig. S5 (a) Nitrogen adsorption/desorption isotherms. (b) Pore size distribution curves of PANI/GO/CNTs (20%, 50%, 80%).

The N_2 adsorption-desorption isotherms showed a H3-type hysteresis loop for PANI/GO/CNT composite films (20%, 50%, 80%), the specific surface area (SSA) values of which were 17.9, 20.6, 40.9 m^2/g, respectively. Their average pore sizes were 22.1, 15.09 and 11.93 nm, respectively. The increase of the SSA may ascribed to the increase incorporation of PANI fibers and the existence of CNTs, which inhibit intense stacking of GO nanosheets.

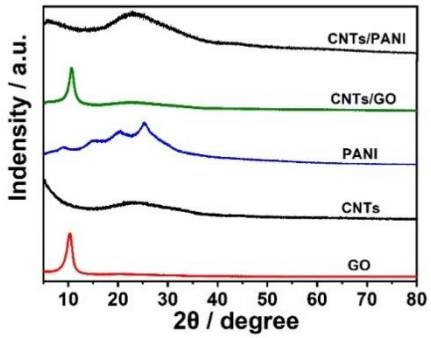

Fig. S6 XRD patterns of GO, CNTs, PANI, CNTs/GO, CNTs/PANI.

The diffraction peaks of PANI/GO/CNTs (20%, 50% and 80%) showed similar tendency with CNTs/GO, CNTs/PANI, indicating that no additional crystalline order was introduced into the composites.

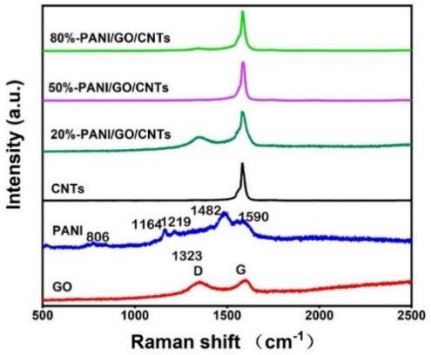

Fig. S7 Raman patterns of GO, CNTs, PANI, PANI/GO/CNTs (20%, 50%, 80%).

GO exhibits characteristic peaks at about 1349 cm^{-1} and 1585 cm^{-1}, corresponding to D and G carbon bands respectively[s1]. It was observed from the Raman spectrum of CNTs produced by the CVD method showed very high G band (1582 cm^{-1}) and very low D band (1334 cm^{-1}), indicating that the structure of the material is high and the defect points can be ignored[s2, s3]. For pure PANI, the typical characteristic peak values at 806, 1164, 1219, 1482, and 1590 cm^{-1} corresponded to the C-H expansion vibration of the quinoid ring, the C-H expansion vibration of the benzene ring, the telescopic vibration of $C\text{-}N^{+}$, the C=C expansion vibration of the quinoid ring and the C=C expansion vibration of the benzene ring of PANI, respectively[s4, s5]. For 20%-PANI/GO/CNTs, 50%-PANI/GO/CNTs and 80%-PANI/GO/CNTs, the Raman spectrum represent obvious D and G carbon bands, the characteristic peak of PANI was not clearly exhibited due probably to the peaks of PANI being too weak and/or overlapped with the GO and CNT peaks, as observed in a previous study[s6].

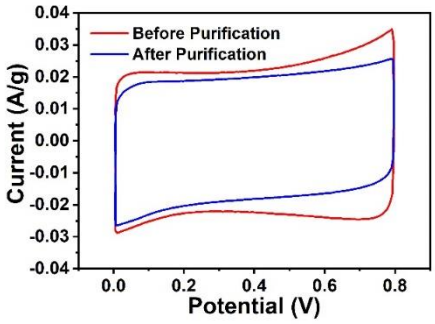

Fig. S8 CV curves of CNTs before and after purification.

In this regard, we measured the CV curves of a spun straight shape CNT fiber before and after purifying by loading the voltage and soaking in 0.1 M of HCl for 12 h and found that the degradation is modest in purified samples[30], indicating that the influence of impurities in CNTs on the electrochemical performance of the composite is not significant.

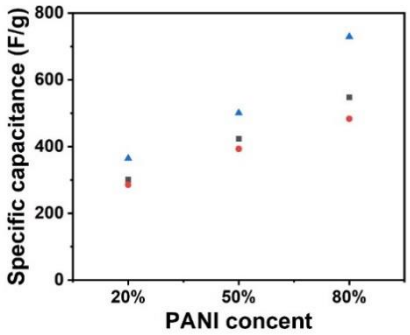

Fig. S9 Specific capacitance based on total mass of PANI, GO and CNTs.

At a current density of 1 A/g, the specific capacitances of the 20%-PANI/GO/CNT, 50%-PANI/GO/CNT, and 80%-PANI/GO/CNT composite film electrodes were 301.1 F/g (120.44 mF/cm^2), 501.2 F/g (200.48 mF/cm^2) and 729.3 F/g (510.51 mF/cm^2), respectively.

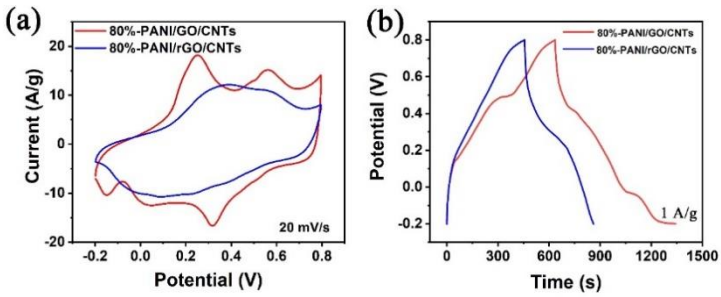

Fig. S10 (a) CV curves and (b) GCD curves of 80%-PANI/GO/CNT composite film and 80%-PANI/rGO/CNT composite film.

The sample of 80%-PANI/GO/CNT composite film electrode exhibited a considerably larger capacitance than 80%-PANI/rGO/CNT composite film electrode. The GCD curves showed that 80%-

PANI/GO/CNT and 80%-PANI/rGO/CNT composite film electrode delivered a specific capacitance of 729.3 F/g and 424.5 F/g in a current density of 1 A/g, respectively.

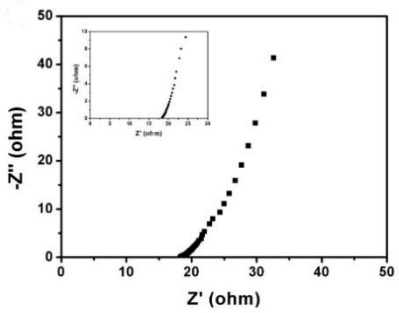

Fig. S11 Nyquist plots of the 80%-PANI/GO/CNT film symmetric supercapacitor.

The EIS curve showed an *Rs* of 17.18 Ω and the impedance curve reflected the trend parallel to the imaginary axis indicating an ideal capacitance behavior.

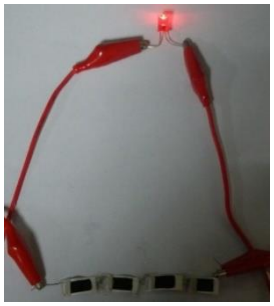

Fig. S12 Image of the 80%-PANI/GO/CNTs composite film-like supercapacitor lighted a LED.

Besides, our film-shaped SSCs could be readily connected in series to light a red LED (1.8 V and 0.06 W) stably for a period of 50 s.

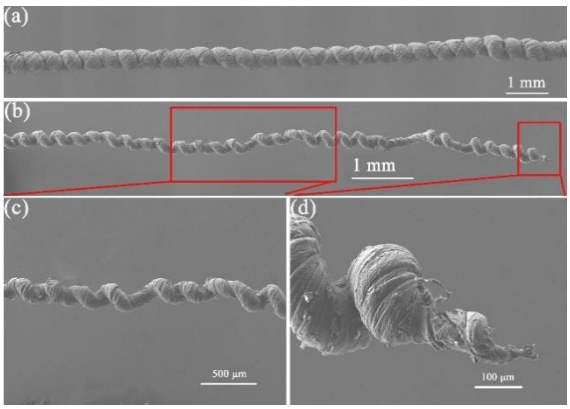

Fig. S13 (a) SEM image of the original helical fiber before stretching, (b, c) SEM images of the composite helical fiber after stretching, (d) the fracture of helical fiber.

We have examined the evolution of microstructure when the composite helical fiber was stretched to tensile strains as large as 120% until fracture. During continuous stretching, the spiral loops were gradually stretched and separated from each other, and this deformation of the helix structure brought

the fibers good tensile properties especially large fracture strains.

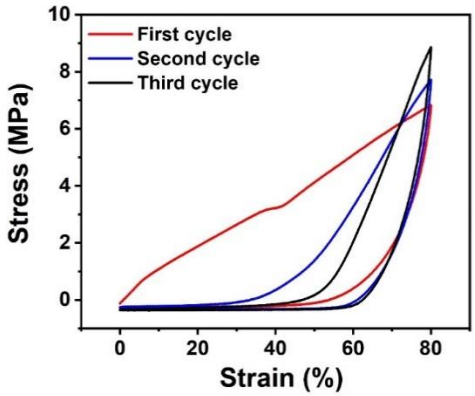

Fig. S14 The static cyclic tests of 80%-PANI/GO/CNTs composite helical fiber covered by gel electrolyte at predefined strain of ε=80%.

We also performed the static cyclic tests of 80%-PANI/GO/CNTs composite helical fiber covered by gel electrolyte at predefined strain of ε=80%, there can observed a large hysteresis in the σ-ε curve.

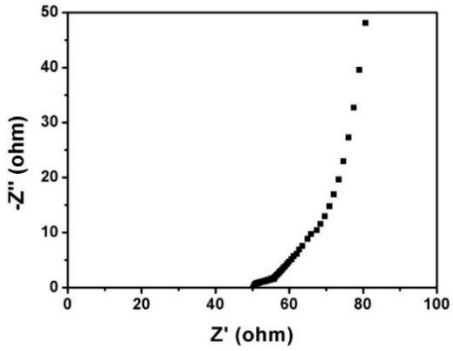

Fig. S15 Nyquist plots of the 80%-PANI/GO/CNT fiber symmetric supercapacitor.

Fig. S15 showed the EIS curve of the 80%-PANI/GO/CNTs composite fiber-like symmetric supercapacitor, showed an *Rs* of 50.25 Ω and the impedance curve parallel to the imaginary axis indicating an ideal capacitance behavior.

Table S1 Comparison of the electrical conductivity of the composite material

Material	R (Ω)	S (cm×μm)	L (m)	Conductivity (S/m)
GO	---	1×10	1×10^2	Non conductive
PANI	20.8×10^3	2.5×135	1×10^2	0.14
20%-PANI/GO/CNTs	75	1×55	1×10^2	242.4
50%-PANI/GO/CNTs	55	1×62	1×10^2	293.3
80%-PANI/GO/CNTs	26	1×71	1×10^2	541.7

The electrical conductivity of composites measured by Digital multimeter, S (m^2) is cross-

sectional area, L (m) is effective length, R (Ω) is resistance. The resistivity of composites calculated from: $\rho = \frac{RS}{L}$, the electrical conductivity σ (S/m) of composites calculated from: $\sigma = \frac{1}{\rho}$.

Comparison of the electrical conductivity of the composite material before and after the introduction of CNTs was shown Table S1. The results showed that the conductivity of the composites increased significantly after the introduction of CNTs in the composites, which was attributed to the existence of three-dimensional conductive networks constructed by the presence of CNTs.

Table S2 Comparison of the electrochemical performance and flexibility of the supercapacitor

electrode	specific capacitance (film-like SC)	specific capacitance (fiber-like SC)	cycling performance	flexibility	Ref.
PANI/GO/CNTs	89.5 F/g	71 F/g	80% for 5000 cycles	93.5% for bending 1000 cycles 98.1% for stretching 80%	**This work**
MoS_2-rGO/MWCNT		3.8 F/cm^3	---	100% for bending 7000 cycles	47
carbon/MnO_2		2.5 F/cm^3	84% for 10000 cycles	---	48
MWCNT		13.5 F/cm^3	108% for 10000 cycles	100% for bending 10000 cycles	49
C@MnO_2/ZnO		0.52 F/cm^3	87.5% for 10000 cycles	---	50
CNT/PANI	184.6 mF/cm^2	---	100% for 500 cycles	---	s7
CNT/PANI	---	255 F/g	69% for 10000 cycles	93.8% for bending 1000 cycles 97.9% for stretching 100%	s8
CNT/PANI	---	272.7 F/g	96.4% for 2000 cycles	---	s9
PANI-ZIF-67	35 mF/cm^2	---	80% for 2000 cycles	---	s10
PANI	237.5 mF/cm^2	---	95.2% for 2000 cycles	91% for bending 180°	s11
NG-PAA/PANI	68 F/g	---	83.2% for 2000 cycles	---	s12

As seen in literature, the specific capacitance range of the previously reported solid-state supercapacitors based on PANI (or its composite) electrodes was 35-237.5 mF/cm^2. In comparison, the specific capacitance of our device made of 80%-PANI/GO/CNTs composite films and PVA/H_3PO_4 gel electrolyte was 89.5 F/g (179 mF/cm^2), which is not very high, with relatively good capacitance retention of approximately 80% over 5000 cycles. Nevertheless, our work demonstrated both film and fiber-shaped solid state supercapacitors can be fabricated from the same CNT/GO/polymer based composite material. Thus, we have shown here a multi-form supercapacitor, whereas previous studies were focused only on a single-form device (either film or fiber). The ability to achieve multi-form is a distinct advantage enabled by the layered composited structure with interpenetrated CNT network and active materials, designed and realized in our roller dipping method. Furthermore, the resulting spiral fiber was capable of self-stretching without relying on external substrate such as polymer elastomers, which was different with straight or substrate-anchored fibers reported previously[49]. In addition, both film-like and fiber-like supercapacitors exhibited excellent electrochemical stability under deformation,

bending, and stretching, respectively, indicating their potential for practical application in flexible energy storage devices.

Reference

1. P.B. Liu, Y. Huang, J. Yan, Y.W. Yang, Y. Zhao, Construction of CuS nanoflakes vertically aligned on magnetically decorated graphene and their enhanced microwave absorption properties, *ACS Appl. Mater. Interfaces* 8 (8) (2016) 5536-5546.
2. B. Li, H. Cao, J. Shao, M. Qu, J.H. Warner, Superparamagnetic Fe_3O_4 nanocrystals@graphene composites for energy storage devices, *J. Mater. Chem.* 21 (2011) 5069-5075.
3. T.Y. Liu, A.B. Davijani, J.Y. Sun, S. Chen, S. Kumar, Hydrothermally oxidized single-walled carbon nanotube networks for high volumetric electrochemical energy storage, *Small* 12 (25) (2016) 3423-3431.
4. A. Tiwaria, R. Kumar, M Prabaharan, R.R. Pandey, P. Kumari, A. Chaturvedi, A. Mishra, A. K. Polym. Nanofibrous polyaniline thin film prepared by plasma-induced polymerization technique for detection of NO_2 gas, *Polym. Advan. Technol.* 21 (9) (2010) 615-620.
5. L. Li, Z. Y. Qin, X. Liang, Q.Q. Fan, Y.Q. Lu, W.H. Wu, M.F. Zhu, Facile, Fabrication of uniform core−shell structured carbon nanotube−polyaniline nanocomposites, *J. Phys. Chem.* 113 (14) (2009) 5502-5507.
6. S. Liu, X.H. Liu, Z.P. Li, S.R. Yang, J.Q. Wang, Fabrication of free-standing graphene/polyaniline nanofibers composite paper via electrostatic adsorption for electrochemical supercapacitors. *New J. Chem.* 35 (2011) 369-374.
7. S. Zeng, H.Y. Chen, F. Cai, Y.R. Kang, M.H. Chen, Q.W. Li, Electrochemical fabrication of carbon nanotube/ polyaniline hydrogel film for all-solid-state flexible supercapacitor with high areal capacitance, *J. Mater. Chem. A* 3 (2015) 23864-23870.
8. X.L. Chen, H.J. Lin, J. Deng, Y. Zhang, X.M. Sun, P.N. Chen, X. Fang, Z.T. Zhang, G.Z. Guan, H.S. Peng, Electrochromic fiber-shaped supercapacitors, *Adv. Mater.* 26 (48) (2014) 8126-8132.
9. S.W. Pan, H.J. Lin, J. Deng, P.N. Chen, X.L. Chen, Z.B. Yang, H.S. Peng, Novel wearable energy devices based on aligned carbon nanotube fiber textiles, *Adv. Energy Mater.* 5 (4) (2015) 1401438.
10. L. Wang, X. Feng, L.T. Ren, Q.H. Piao, J.Q. Zhong, Y.B. Wang, H.W. Li, Y.F. Chen, B. Wang, Flexible solid-state supercapacitor based on a metal−organic framework interwoven by electrochemically-deposited PANI, *J. AM. Chem. Soc.* 137 (15) (2015) 4920-4923.
11. H.H. Li, J. Song, L.L. Wang, X.M. Feng, R.Q. Liu, W.J. Zeng, Z.D. Huang, Y.W. Ma, L.H. Wang, Flexible all-solid-state supercapacitors based on polyaniline orderly nanotubes array, *Nanoscale* 9 (193) (2017) 193-200.
12. Y.G. Wang, S.C. Tang, S. Vongehr, J.A. Syed, X.Y. Wang, X.K. Meng, High-performance flexible solid-state carbon cloth supercapacitors based on highly processible N-graphene doped polyacrylic acid/polyaniline composites, *Sci. Rep.*, 6 (2016) 12883.